Journal of Materials Science and Chemical Engineering, 2025, 13(2), 83-98
https://www.scirp.org/journal/msce
ISSN Online: 2327-6053
ISSN Print: 2327-6045

# Effect of Hydroxyapatite Filler in an Aluminosilicate Glass Ionomer Cements

**Md Alamgir Kabir[1], Md Moshiur Rahman[1*], Humayun Kabir[1], Md Moniruzzaman Khan[2], Khokon Hossen[3], Sooraj H. Nandyala[4], Artemis Stamboulis[4]**

[1]Department of Physics, Jahangirnagar University, Dhaka, Bangladesh
[2]Bangladesh Military Academy, Academic Wing, Bhatiary, Chittagong, Bangladesh
[3]Department of Physics and Mechanical Engineering, Patuakhali Science and Technology University, Patuakhali, Bangladesh
[4]School of Metallurgy and Materials, University of Birmingham, Birmingham, UK
Email: *phy_mmr@juniv.edu

**How to cite this paper:** Kabir, M.A., Rahman, M.M., Kabir, H., Khan, M.M., Hossen, K., Nandyala, S.H. and Stamboulis, A. (2025) Effect of Hydroxyapatite Filler in an Aluminosilicate Glass Ionomer Cements. *Journal of Materials Science and Chemical Engineering*, **13**, 83-98.
https://doi.org/10.4236/msce.2025.132006

**Received:** December 28, 2024
**Accepted:** February 23, 2025
**Published:** February 26, 2025



## Abstract

Hydroxyapatite (HA) is widely explored as a biocompatible filler to enhance the mechanical and functional properties of glass ionomer cements (GICs). HA of particle sizes 15 μm and 30 μm were added as a filler into a matrix, composed of calcium aluminosilicate GICs and Poly-acrylic acid (PAA) in varying ratios. The tested ratios were Glass:PAA = 2:1 and Glass:HA:PAA = 2:0.5:1 to improve the mechanical strength of a conventional GIC. Mechanical properties, including compressive, flexural, and diametral tensile strength were studied at different setting times. The compressive strength (CS) was improved with hydroxyapatite addition and prolonged setting time while diametral tensile strength (DTS) did not follow any specific trend. The flexural strength (FS) of the composite cement was increased with increasing setting time regardless of the particle size of hydroxyapatite. The FTIR spectra of hydroxyapatite of particle sizes 15 μm and 30 μm are similar but for HA-GIC composites, the FTIR spectra, the peak around 1460 $cm^{-1}$ are due to C-H and the peak at 1553 $cm^{-1}$ is due to calcium carboxylate with calcium in a bridging mode which would be an excellent material that chemically bonds to the tooth structure, making it effective for both restorative procedures and cavity fillings. Scanning electron microscopy (SEM) microstructural study revealed that the glass particles were wrenched out, which was a cohesive fracture. The X-ray diffraction (XRD) pattern showed that the hydroxyapatite has a crystalline single-phase, hexagonal structure. The sharp peaks between the 2-theta range of 30 - 40 degrees are the same as in enamel powder. The spectra indicate the pure set cement as amorphous since there is no prominent peak, but with the addition of hydroxyapatite filler, the peak in the 2-theta range of 20 - 35 degrees is ascribed to crystalline apatite structure. The results indicate that

incorporating hydroxyapatite into GIC significantly enhances its mechanical properties and structural integrity, suggesting its potential as an improved material for dental and restorative applications.

## Keywords

FTIR, SEM, EDX, XRD, Hydroxyapatite (HA), Poly-Acrylic Acid (PAA), RBCs, Biomaterials, CS, DTS, FS

## 1. Introduction

The use of biomaterials in dental treatments is intense, and spans several centuries, progressing with advancements in technology and materials sciences. Glass ionomer cements (GICs) were introduced in the early 1970s as a revolutionary material that chemically bonds to the tooth structure and releases fluoride, making it an effective material for both restorative procedures and cavity prevention. GICs became effective in pediatric dentistry and for patients prone to caries due to their remineralizing properties [1]. In the 1980s and 1990s, Ceramic materials like zirconia and alumina emerged for dental crowns, bridges, and implants due to their superior aesthetic qualities, strength and biocompatibility, and ability to mimic the translucency of natural teeth. However, these materials are poor in color stability, have high polymerization shrinkage, lack bonding to tooth structure, and have a large thermal expansion coefficient. Acrylic resin-based composites (RBCs) were introduced mid-20th as an aesthetic alternative to dental amalgam. Still, they exhibited poor mechanical properties, high polymerization shrinkage, and inadequate wear resistance, which limited their uses. Silica-based filler particles were incorporated into the resin matrix to improve strength, wear resistance, and thermal properties [2] [3]. RBCs placement requires complex clinical protocols, including isolation from moisture, precise layering, and curing techniques, its shrinking properties during curing, may cause microleakage, marginal gaps, and impaired post-operative sensitivity [4]-[6]. RBCs are less durable than amalgam in high-load-bearing restorations, with a higher risk of wear and fracture over time [7]. They are more expensive than traditional materials like amalgam and exhibit incomplete polymerization that may retain unreacted monomers and subsequently affect biocompatibility. Moreover, their coefficient of thermal expansion differs from natural tooth structure, which may lead to marginal discrepancies with temperature changes and they can absorb stains from food, beverages, and tobacco over time, therefore, compromising aesthetics [8]-[10].

Several new composites based on bis-acrylamide and monomers such as spiro-ortho-carbonates, vinyl-cyclo-propane, and silorane (a combination of siloxane and oxirane moieties) have been introduced that exhibit less shrinkage [11]-[15]. Smith (1967) developed zinc poly-acrylate cement with zinc-oxide powder and a PPA solution [16], later several metal oxides and fillers were added to poly-

electrolyte cement, and these poly-acrylate cements were able to bind with the tooth structure as well as their physical poly-electrolyte cements were improved with low toxicity [17]. Although poly-acrylate cements have novel adhesive properties, they are opaque, non-aesthetic, and take a long time to set. GICs, made of glass powder and 45% aqueous solution of PAA, evolved in London (1969) but exhibited poor mechanical properties [1] [18]. The improvement of GICs has become a challenge among the scientific community since the beginning. Metal-reinforced GICs like "Miracle Mix" and "Cermet" were developed by incorporating a silver alloy powder in the glass powder, to improve wear resistance [19] [20]. To overcome the moisture sensitivity of the acid-base reaction in GICs, a new generation of command-set resin-modified glass-ionomer cements (RMGIC) was developed exhibiting improved mechanical properties. Now, GICs are translucent, release fluoride, form a chemical bond to the tooth structure, elicit a less unfavorable response, and have a low coefficient of thermal expansion as compared with other restorative materials [21] [22].

Recently (2016) hydroxyapatite (HA) synthesized filler composite cements were studied and found that the addition of 5 wt% (HA-$Ca_{10}(PO_4)_6(OH)_2$) with conventional cements and 7 days storage in water has a positive effect on the mechanical properties [23]. Hydroxyapatite (HA) is biocompatible and bioactive [24], and is extensively used in orthodontic and dental applications since it is a major ingredient of human bone and teeth. HA was used as filler in GICs for improving properties such as compressive strength, diametral tensile strength, and flexural strength [23] [25]. The principal aim and objective of this research are to study the effect of hydroxyapatite (HA) as filler in experimental aluminosilicate GICs and to improve their mechanical properties. A comparison between the conventional experimental cement properties with the properties of the modified hydroxyapatite cement composite especially when hydroxyapatite of different particle sizes was used, was also conducted. XRD study was conducted to observe crystallinity in the composite cements. FTIR was conducted to investigate the change in the chemical bonding in composite cements. SEM studies were performed to observe the fracture type of GICs after the addition of hydroxyapatite. Mechanical properties such as compressive strength, diametral tensile strength, and flexural strength were investigated to study the effect of hydroxyapatite addition on the bulk properties of GICs.

## 2. Methodology

### 2.1. Sample Preparation

Calcium aluminosilicate glass ($4.5SiO_2$-$3Al_2O_3$-$1.5P_2O_5$-CaO-$2CaF_2$) was prepared in the laboratory by an established melt quenching route [26]. Poly-acrylic acid solution (PAA) ($C_3H_4O_2$) was provided by BASF plc, Cheshire, UK. The analytical grade Hydroxyapatite (HA-$Ca_{10}(PO_4)_6(OH)_2$) of particle sizes 15 μm and 30 μm, was purchased from the chemical company Teknimed, France. Three types of glass ionomer cements GIC, 15HAGIC and 30HAGIC were prepared using the ratio of

powder and liquid as Glass:PAA = 2:1 and Glass:HA:PAA = 2:0.5:1. The powder and the polymer liquid were mixed by a UHMWPE spatula on a PMMA mixing plate within 60 seconds and then cast into Teflon molds onto a steel plate. The steel mold was clamped using a G clamp and the GICs pastes were allowed to set for 60 minutes in an air oven at 37˚C. The molds were then unclamped and all samples were placed into deionized water in glass beakers, which then were stored in a water bath (Thermo Fisher Scientific Inc., Waltham, United States) at 37˚C. The samples were then kept for different aging periods and tested.

## 2.2. Fourier Transform Infrared (FTIR) Spectroscopy

Three different types of cement namely LG26, 15HA, and 30HA were mixed homogeneously with KBr and were ground by a mortar and pestle to further reduce the particle size because the scattering of the infrared beam by larger particle size creates the sloping baseline of the spectrum. Evaporating the KBr, a standard pellet of all the samples was prepared for FTIR. The Nicolet FTIR spectrometer (Magna-IR860) coupled with a deuterated triglycine sulphate (DTGS) detector, was used for FTIR spectroscopy studies. The spectra were collected by transmission infrared source with evolved packet system mode with a speed of 0.6329 $ms^{-1}$. The frequency ranges 400 - 4000 $cm^{-1}$ and a resolution of 0.4821 $cm^{-1}$ was set up with 100 scans over 15 minutes. All the spectrum was filtered *i.e.*, the background noise was eliminated by subtraction.

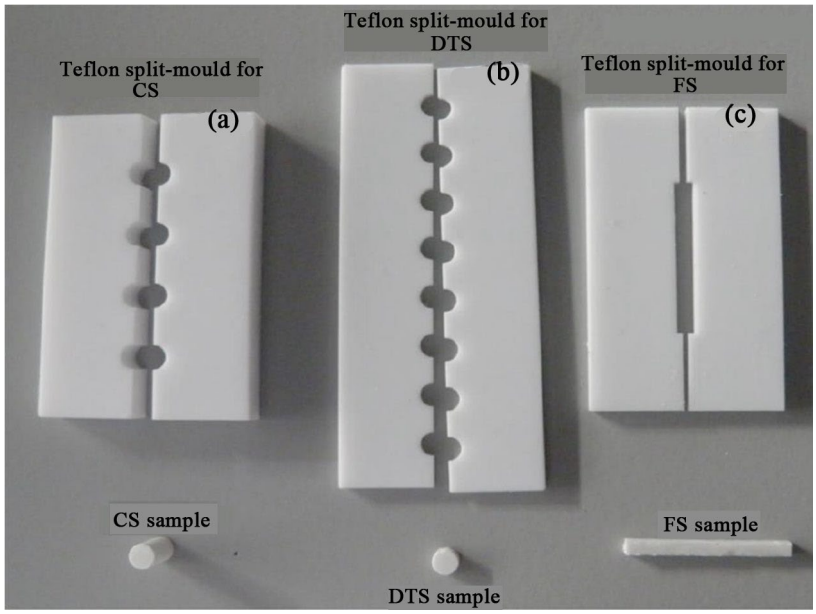


**Figure 1.** (a) Four sample Teflon split mold for CS; (b) Eight sample Teflon split mold for DTS; (c) One sample Teflon split mold for FS measurements.

## 2.3. XRD Studies

X-ray powder diffraction study was done for LG26, GIC, 15HAGIC, and 30HAGIC by Equinox XRD machine (model number 3000) with Cu-K$\alpha$ radiation. The LG26

powder was taken after sieving to investigate whether there was any crystallization occurring during quenching. The 2-theta range was 10 - 90 degrees with a resolution of 0.02983 degrees, with 35 kV - 25 mA throughout the experiments. The total scan time for the whole 2-theta range was 7200 seconds. The JCPDS database was used as a reference to determine the phases. The peak position was identified by Match software.

### 2.4. Scanning Electron Microscopy (SEM) Studies

The particle size and distribution of raw powder of hydroxyapatite and glass and the fracture surface after flexural test of different GICs (GIC, 15HAGIC, 30HAGIC) were studied by electron microscope. The SEM machine used here was a high-resolution JEOL 6060 (Philips Co. Japan) operated at 10 keV operating voltage. The cylindrical-shaped samples were used to study the fracture surface of GICs.

### 2.5. Mechanical Characterization of GICs

Several mechanical properties like **compressive strength (CS)**, **diametral tensile strength (DTS)**, and **flexural strength (FS)** of different glass ionomer cement were investigated by Instron mechanical testing machine (Model-1195) and compared with British Standard (BS) according to the requirement of American Dental Association (ADA) specification [27] [28]. **Figure 1** shows the Teflon split mold, prepared cylindrical samples of (a) dimension 4 ± 0.1 mm in diameter and 6 ± 0.1 mm thickness for CS (b) dimension 4 ± 0.1 mm of diameter and 2 ± 0.1 mm in thickness for DTS and (c) dimension 25 ± 0.1 mm in length and 2 ± 0.1 mm in width and FS measurements. **CS** was assessed by 5 kN load with a cross-head speed of 1 mm/min using Equation (1), **DTS** was measured according to diametral compression of 1kN load, and a crosshead speed of 1mm/min, using Equation (2) [27]. **FS** was studied by applying 500 N load with a cross-head speed of 1 mm/min, using formula (3) [27] [28].

$$CS = \frac{4 \times p}{\pi \times d^2} \tag{1}$$

$$DTS = \frac{2 \times p}{\pi \times d \times T} \tag{2}$$

$$FS = \frac{3 \times F \times l}{2 \times b \times h^2} \tag{3}$$

Where $p$ is the maximum applied load at the specimen, $d$ is the diameter of the cylindrical sample. For *FS*, $F$ is the maximum load at fracture of the sample, $l$ is the distance between two supports, $b$ is the width of the specimen, and the thickness of the specimen is $h$.

## 3. Results

The mechanical properties such as CS, DTS, and FS of the GICs were investigated with different aging times. All of the data presented for mechanical properties are

average values of at least 15 samples. FTIR analysis was performed for investigation of the molecular structure of GICs and its ingredient. The glass particle morphology was studied by SEM. XRD was performed to investigate the crystallinity of the cements and their components. On a trial basis prepared LG26 glass was ground using specialized grinding equipment (MODEL T750K), by using a pestle and mortar, and finally by TEMA mill, and the particle size was measured by a particle size analyzer. All analyzed curves follow a normal distribution, which signifies the study's accuracy, but only TEMA mill ground one was studied for proper size (10 - 25 μm). Similarly, the particle size distribution for 15 HA and 30 HA was also done (the average particle size of 15 HA was 13.72 μm and for 30 HA it was 24.15 μm). The liquid-to-powder ratio was optimized 2:1 for homogeneous mixing with lower viscosity to cast in a mold.

### 3.1. Fourier Transform Infrared (FTIR) Analysis

The FTIR study of every single element and different GICs (GIC, 15HAGIC, 30HAGIC) like PAA, LG 26, 15HA, 30HA, 15HAPAA, and 30HAPAA was done and the major peaks in FTIR spectra are shown in **Figure 2**.

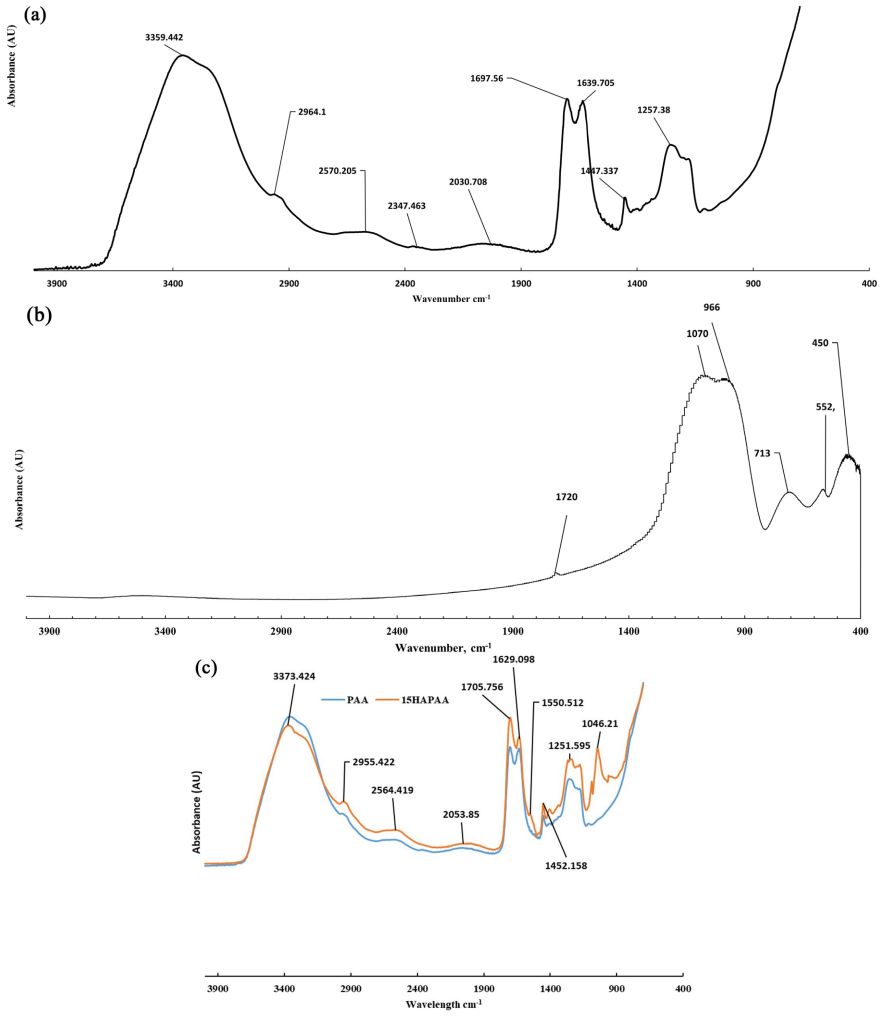

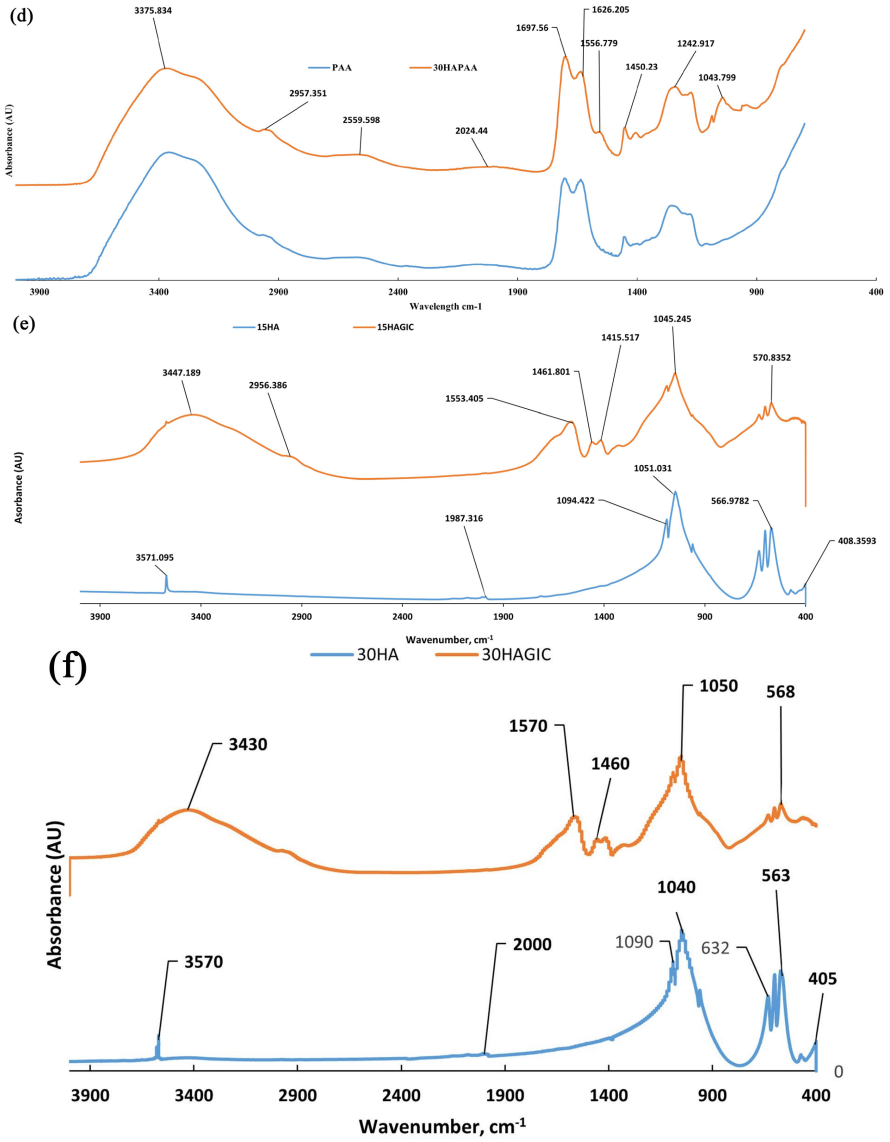


**Figure 2.** FTIR spectra (a) 40% of PAA solution; (b) LG26 glass; (c) 15HAPAA liquid (yellow) and PAA (blue); (d) 30HAPAA liquid (yellow) and PAA (blue); (e) 15HA(blue) and 15HAGIC (yellow); (f) 30HA(blue) and 30HAGIC (yellow).

In the FTIR spectrum for 40% PAA solution, as shown in **Figure 2(a)**, the main absorption peak at 1697 $cm^{-1}$ was due to carbonyl (C = O) stretching vibrations [29]-[31]. The inter- and intra-layer stretching vibrations of H-bonded O-H are represented by the absorption band at around 3359 $cm^{-1}$ [32]. The monomer and PAA's C-H scissor vibrations peak appeared at 1447 $cm^{-1}$ and the stretching vibration of C-O was observed at 1257 $cm^{-1}$ [29]. The FTIR spectroscopy analysis of ion-leachable glass (LG 26) powder is shown in **Figure 2(b)**. The peak at 450 $cm^{-1}$ is associated with stretching vibrations of Si-O-Si [33]. P-O bending and Si-O-Al stretching vibrations are associated with the peak at 552 $cm^{-1}$ [34]. The stretching vibrations of Al-O bond is represented by the peak at 713 $cm^{-1}$ [35]. The peaks at 966 $cm^{-1}$ and 1070 $cm^{-1}$ are associated with Si-O stretching and P-O bonds [33]

[36]. The FTIR spectrum of hydroxyapatite of particle sizes 15 μm and 30 μm is similar (not included here) but compared in **Figure 2(e) and (f)** blue curve. The peak at 3571 $cm^{-1}$ is due to absorbed water and hydroxyl vibrations. Vibrations of $PO_4$ are associated with the peak at 1041 $cm^{-1}$. The peaks at 400 and 472 were phosphate $\nu_2$ vibrations. The peak at 1400 $cm^{-1}$ is due to carbonate contamination [37]. **Figure 2(c)** shows the FTIR spectrum of 15HAPAA (15HA:PAA = 0.5:1.0) liquid (yellow) is compared with PAA (blue) where the two main peaks at around 1600 and 1700 $cm^{-1}$ are still similar in the blended liquid. The only noticeable peak in 15HAPAA blend liquid different from PAA peaks is at 1550 $cm^{-1}$ which is due to calcium carboxylate with calcium in a bridging state [38]. Like **Figure 2(c)**, **Figure 2(d)** show a similar result for 30HAPAA liquid (15HA:PAA = 0.5:1.0). **Figure 2 (e)** shows the FTIR spectra of 15HA powder and 15HAGIC cement after 4 weeks of setting. **Figure 2(f)** shows the FTIR spectra of 30HA powder and 30HAGIC cement after 4 weeks of setting. In 15HAGIC and 30HAGIC the peaks are shifted slightly to the right. From 800 $cm^{-1}$ to 1300 $cm^{-1}$ there is a broad peak with a major peak at 1045 $cm^{-1}$ in 15HAGIC and at 1050 $cm^{-1}$ in 30HAGIC because of Si-O stretching vibrations. The peaks at 570 $cm^{-1}$ in 15HAGIC and 566 $cm^{-1}$ in 15HA are congruent peaks ascribed to phosphate $\nu_4$ vibrations. Similarly, the peak at 568 $cm^{-1}$ in 30HAGIC and 563 $cm^{-1}$ in 30HA are due to phosphate ν4 vibrations [37]. There might be some unreacted PAA in the cement and thus peaks around 1460 $cm^{-1}$ in both 15HA and 30HA are due to C-H scissoring of PAA and monomers [29]. The peaks at 1553 (**Figure 2(e)**) and 1570 (**Figure 2(f)**) are due to calcium carboxylate with calcium in bridging mode [38].

### 3.2. Mechanical Properties

**CS** as shown in the bar diagram, **Figure 3(a)**, increased with time and the maximum value of average compressive strength was found to be about 86 MPa for 15HAGIC after 4 weeks from mixing. Finally, for 30HAGIC, the **CS** increased up to two weeks after mixing but decreased after that. It is worth noticing, that the cements containing HA with larger particle sizes showed higher **CS** in the first two weeks but lower **CS** after that, compared with the cements containing smaller particle sizes in HA. In this test, the alpha value was taken 0.05, where $p > 0.05$ has no significant difference between the two groups of cements but when $p < 0.05$ has a significant difference between the two groups of cements. From this t-test result, it is seen that the two sets of comparison groups GICs to 30HAGIC and 15HAGIC to 30HAGIC have significant differences as both groups had p-values of less than 0.05. The **CS** of GIC and 15HAGIC are not significantly different as the p-value was greater than 0.05.

**DTS** was assessed, as shown in **Figure 3(b)**, by an Instron machine by applying compressive forces along the diameter adopting the British Standard Institution rule [27]. From the **Figure 3(b)**, it is clear that the **DTS** of conventional GIC reached the highest value of about 15 MPa in 168 hours of setting. After 168 hours

of aging, the **DTS** was decreased. The **DTS** of 15HAGIC continued to increase with time and for 30HAGIC, **DTS** was increased up to 3 weeks of aging, after that it was decreased. The results showed that the **DTS** was notably lower than the CS as the GICs are brittle materials, and crack propagates easily due to tensile loading than compression loading. In this test, shear stress arose between the specimen and the flat metal disk of the testing machine. As the shear failure was followed by tensile failure, the cements broke with a significantly small amount of load. The confidence level of the t-test was 95%. The t-test result of diametral tensile strength shows that there was no significant difference among different groups of samples as the p values were all clearly greater than 0.05.

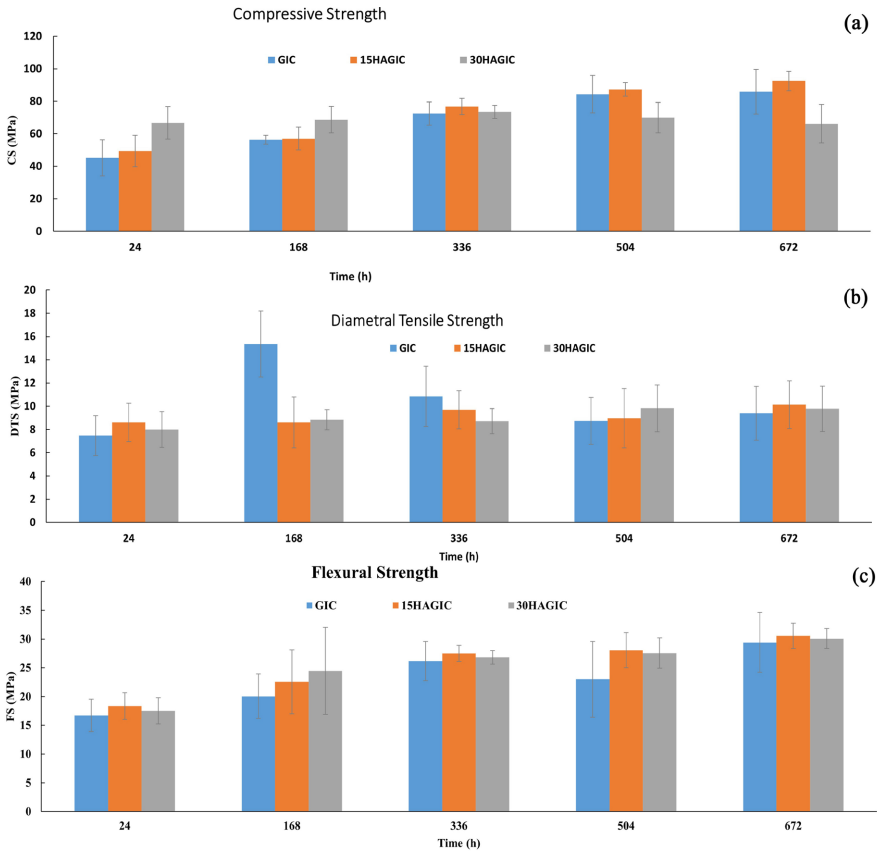


**Figure 3.** The mechanical properties of GIC, 15HAGIC, and 30HAGIC with time (a) compressive strength; (b) diametral tensile strength; (c) flexural strength.

**FS** of all cements increased with aging time except the conventional GIC. The **FS** of GICs dropped in the 3rd week and increased again in the 4th week after mixing. 15HAGIC showed an increasing pattern of **FS** trend for all aging times. During the aging period of four weeks, the flexural strength for 15GIC was the highest except in 168 hours. 30HAGIC also showed an increasing trend throughout aging time. Therefore, the t-test shows that the flexural strength of the two cements had no significant difference (since $p > 0.05$). It is noticeable that the general trend is increasing flexural strength for all individual cements.

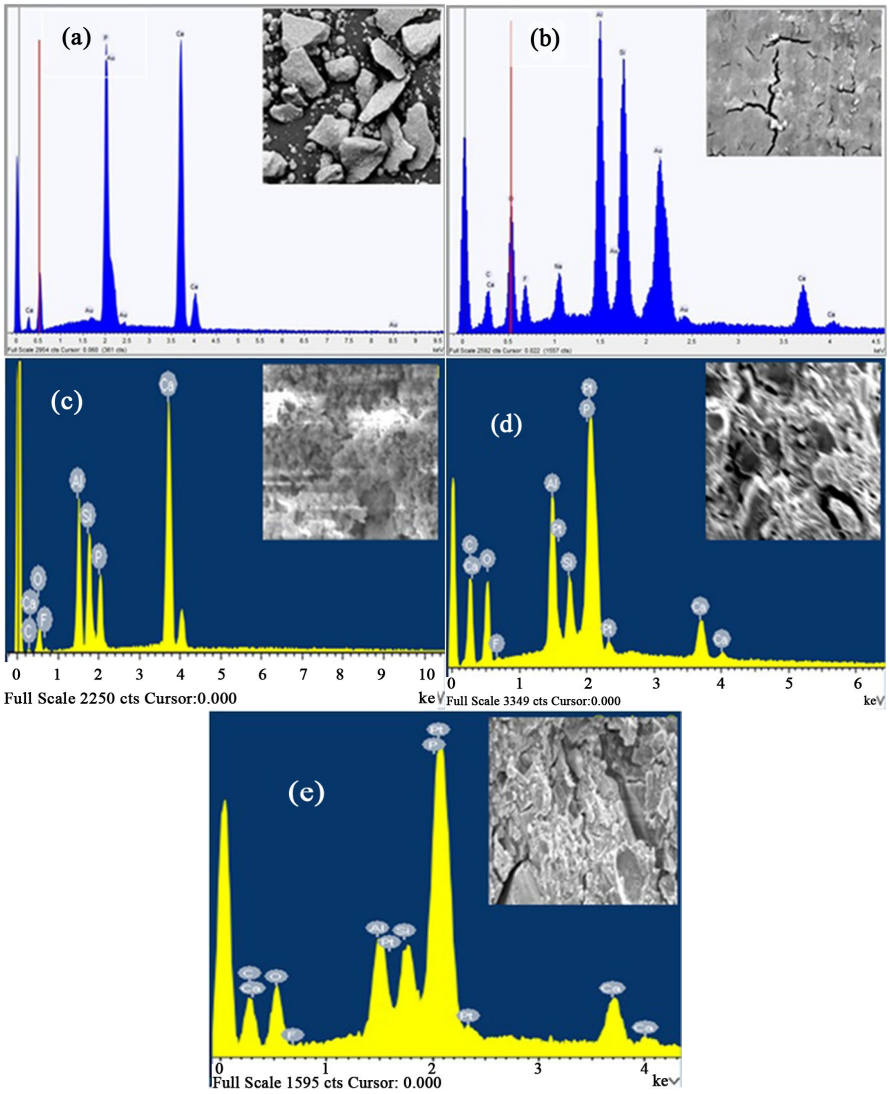


**Figure 4.** EDX spectra and SEM image (inset) (a) HA (b) GIC (c) LG26 glass (d) Pure GIC (e) 30HAGIC.

### 3.3. Surface Morphology and Elemental Analysis

The EDX spectra and SEM image(inset) of the HA (grain size 15 - 30 μm), and GICs are shown in **Figure 4(a)**. The EDX shows that the major ingredients of hydroxyapatite are calcium and phosphorus. The EDX spectra of pure hydroxyapatite confirmed the calcium-to-phosphorus ratio as 1.67. In **Figure 4(b)**, the SEM image(inset) of a cylindrical GIC sample shows that the outer surface has a lot of cracks due to dehydration. In the case of SEM imaging, vacuum water evaporates, and cracks are formed, therefore SEM is not a standard technique for microstructural characterization of GIC. The microscopic anatomy of GICs revealed that the fractured surface of cement specimens consists of both large and small glass particles which can readily be distinguished from the polymer matrix. **Figure 4 (c)** shows the SEM image (inset) and EDX spectrum of LG 26 with their composition. **Figure 4 (d)** EDX spectrum and the SEM of pure GICs. Similarly, **Figure**

4(e) shows the SEM image and EDX spectrum of 30HAGIC. Figure 5 shows the fracture surface of flexural samples of pure GIC, 15HAGIC, and 30HAGIC. From, these figures it is clear that the glass particles were pulled out of the fracture surface under the applied bending force.

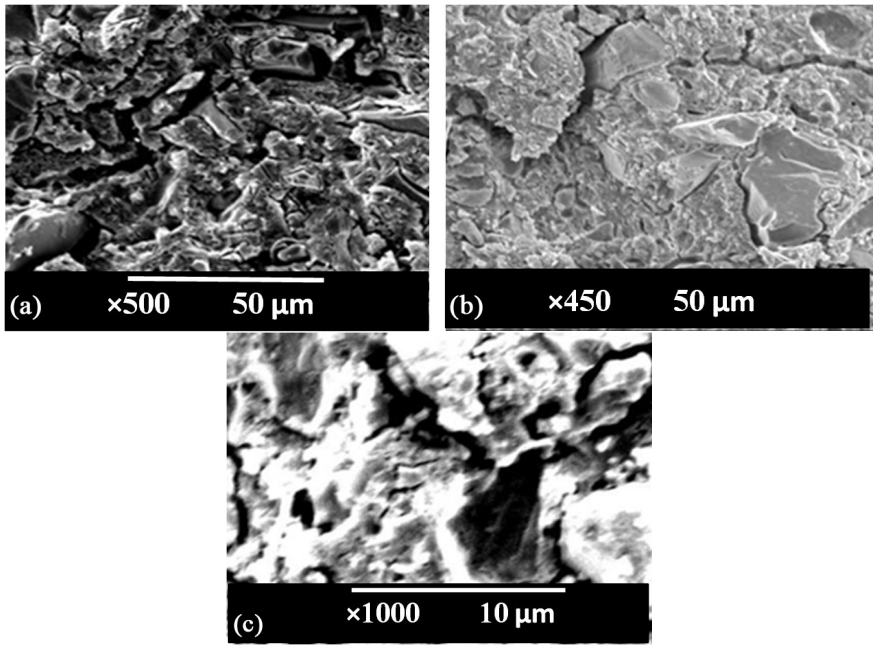


Figure 5. SEM of fracture surfaces of (a) pure GIC; (b) 15HAGIC; (c) 30HAGIC.

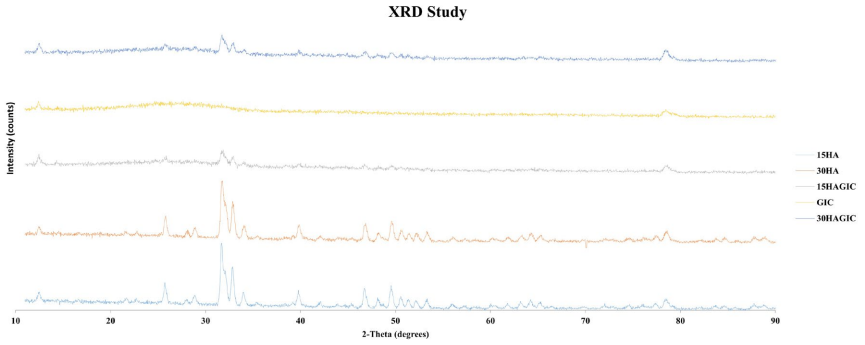


Figure 6. XRD pattern of Pure GICs, HA and HA-GIC composites.

## 3.4. XRD Studies

Figure 6 depicts the X-ray diffraction pattern of 15 µm hydroxyapatite, 30 µm hydroxyapatite, pure GIC, 15HAGIC, and 30HAGIC respectively. This pattern indicates that the hydroxyapatite has a crystalline single phase. Its structure is hexagonal. The sharp peaks are between 30 and 40 degrees, in the 2-theta range and these peaks correspond to JCPDS 9-0432 file. These peaks are also the same as observed in enamel powder. From these spectra, it is evident that the pure set cement was amorphous as there is no prominent peak. After adding hydroxyapatite filler, some peaks are observed in 15HAGIC and 30HAGIC cements associated

with the presence of hydroxyapatite. The peaks in HAGIC are shifted to the right compared to the pure HA. The peak in the 2-theta range of 20 - 35 degrees is ascribed to crystalline apatite structure.

## 4. Discussions

Inferential statistics such as the T-test, allow us to make inferences about the population beyond our data. This test checks if two means are reliably different from each other. The p-value is the probability that the pattern of data in the sample could be produced by random data. The p-value for each t-value also depends on the sample size. Bigger samples make it easier to detect differences. The significance level, $\alpha = 0.05$; probability of rejecting the null hypothesis when it is true. Therefore, when $p < 0.05$ there will be a significant difference between data, and when $p > 0.05$ there will be no significant difference between data. The mechanical properties like **CS**, **DTS**, and **FS** are in general increasing by reinforcement with hydroxyapatite up to a certain aging time (30 HA - 2 week) and then decreasing. **DTS** was not influenced by the addition of hydroxyapatite and generally the values increased slightly for all cements except the conventional experimental cement without hydroxyapatite. The reinforced particle size was 15 μm and 30 μm and therefore mechanical properties were not enhanced significantly. The t-test result (p-value < 0.05) reveals that the compressive strength for comparison groups GICs to 30HAGIC and 15HAGIC to 30HAGIC are significantly different. The **CS** for 15HAGIC was in the range 66 - 92 Mpa, whereas for GICs it was 45 - 85 MPa. The **FS** of controlled GICs was not stable as the standard deviation was higher than composite cements. The **FS** of composite cements is increased but not significant since the t-test result showed the p-value is greater than 0.05. Therefore, the replacement of glass by HA has a moderate effect on the FS of GICs. Furthermore, nano-hydroxyapatite may also enhance the mechanical properties better than micro-size hydroxyapatite filler as reported by Barandehfard [23]. The fracture is visible in all flexural samples, under tensile stresses due to microstructural imperfections or the presence of bubbles which would be the major causes of the clinical failure of dental restoratives. In most commercial cements, the glass compositions are unknown and therefore it is difficult to comment on the setting duration. But in this study, the glass was prepared in our laboratory by strictly flowing the ratio of the ingredients. The reactions among PAA, $Ca^{2+}$, and $Al^{3+}$ were not completed after 24 hours and for that, the mechanical properties were the lowest after 24 hours of setting [23]. After 1 day, the mechanical properties were improved because of the reaction with $Ca^{2+,}$ and the carboxylate group of PAA progressed to complete. FTIR Spectroscopy reveals the chemical structure of PAA-HA-GICs composites at the molecular level [39]. The single peak at 1550 $cm^{-1}$ is attributed to calcium carboxylate with calcium in bridging mode [38]. Although conventional SEM is not ideal for studying the microstructure the microscopic observation of GICs revealed that the fractured surface of cement specimens consists of both large and small glass particles which can readily be

distinguished from the polymer matrix. It is possible to overcome the difficulties by the use of ESEM, cryo-SEM, or TEM micrographs but these are excluded in this study due to the limitation of accessibility.

## 5. Conclusion

In the present study, the molecular structure, particle morphology, and mechanical and physicochemical properties of pure glass ionomer and hydroxyapatite-reinforced glass ionomer cements were investigated. The hydroxyapatite-containing cements showed higher compressive strength (92.45 MPa), and higher flexural strength (30.55 MPa) but lower diametral tensile strength. The detailed chemical bonding such as cross-linking in the cements was revealed by the FTIR study. The XRD studies showed that there was no significant change in the crystalline properties of the composite cement and that in GICs there was negligible crystal structure. For restorative glass composites, acid or heat treatment, mechanical testing for a long time is required. Real-time FTIR could provide a better insight into the crystal.

## Conflicts of Interest

The authors declare no conflicts of interest regarding the publication of this paper.

## References

[1] Wilson, A.D. and Kent, B.E. (1971) The Glass-Ionomer Cement, a New Translucent Dental Filling Material. *Journal of Applied Chemistry and Biotechnology*, **21**, 313. https://doi.org/10.1002/jctb.5020211101

[2] Li, Y., Swartz, M.L., Phillips, R.W., Moore, B.K. and Roberts, T.A. (1985) Materials Science Effect of Filler Content and Size on Properties of Composites. *Journal of Dental Research*, **64**, 1396-1403. https://doi.org/10.1177/00220345850640121501

[3] Ferracane, J.L. (2001) Materials in Dentistry: Principles and Applications. Lippincott Williams & Wilkins.

[4] Ferracane, J.L. (2024) A Historical Perspective on Dental Composite Restorative Materials. *Journal of Functional Biomaterials*, **15**, Article No. 173. https://doi.org/10.3390/jfb15070173

[5] Cardoso, L.S., Oliveira, A.A.D., Barbosa, G.D.M., Ribeiro, M.L.P., Firmiano, T.C. and Veríssimo, C. (2024) Evaluation of Polymerization Shrinkage Stress and Cuspal Strain in Natural and Typodont Teeth. *Brazilian Oral Research*, **38**, e061. https://doi.org/10.1590/1807-3107bor-2024.vol38.0061

[6] Braga, R., Ballester, R. and Ferracane, J. (2005) Factors Involved in the Development of Polymerization Shrinkage Stress in Resin-Composites: A Systematic Review. *Dental Materials*, **21**, 962-970. https://doi.org/10.1016/j.dental.2005.04.018

[7] Davidson, C.L., De Gee, A.J. and Feilzer, A. (1984) The Competition between the Composite-Dentin Bond Strength and the Polymerization Contraction Stress. *Journal of Dental Research*, **63**, 1396-1399. https://doi.org/10.1177/00220345840630121101

[8] Rueggeberg, F.A. (2011) State-of-the-Art: Dental Photocuring—A Review. *Dental Materials*, **27**, 39-52. https://doi.org/10.1016/j.dental.2010.10.021

[9] Krug, R., Droste, L., Schreiber, C., Reichardt, E., Krastl, G., Hahn, B., *et al*. (2024) Long-Term Performance of Ceramic In/-Onlays vs. Cast Gold Partial Crowns—A Retrospective Clinical Study. *Clinical Oral Investigations*, **28**, Article No. 298. https://doi.org/10.1007/s00784-024-05682-7

[10] Pinto, G.D.S., Oliveira, L.J.C., Romano, A.R., Schardosim, L.R., Bonow, M.L.M., Pacce, M., *et al*. (2014) Longevity of Posterior Restorations in Primary Teeth: Results from a Paediatric Dental Clinic. *Journal of Dentistry*, **42**, 1248-1254. https://doi.org/10.1016/j.jdent.2014.08.005

[11] Ikemura, K., Tay, F.R., Endo, T. and Pashley, D.H. (2008) A Review of Chemical-Approach and Ultramorphological Studies on the Development of Fluoride-Releasing Dental Adhesives Comprising New Pre-Reacted Glass Ionomer (PRG) Fillers. *Dental Materials Journal*, **27**, 315-339. https://doi.org/10.4012/dmj.27.315

[12] Van Landuyt, K.L., Snauwaert, J., De Munck, J., Peumans, M., Yoshida, Y., Poitevin, A., *et al*. (2007) Systematic Review of the Chemical Composition of Contemporary Dental Adhesives. *Biomaterials*, **28**, 3757-3785. https://doi.org/10.1016/j.biomaterials.2007.04.044

[13] Tay, F.R. and Pashley, D.H. (2004) Resin Bonding to Cervical Sclerotic Dentin: A Review. *Journal of Dentistry*, **32**, 173-196. https://doi.org/10.1016/j.jdent.2003.10.009

[14] Santini, A. and Miletic, V. (2008) Comparison of the Hybrid Layer Formed by Silorane Adhesive, One-Step Self-Etch and Etch and Rinse Systems Using Confocal Micro-Raman Spectroscopy and Sem. *Journal of Dentistry*, **36**, 683-691. https://doi.org/10.1016/j.jdent.2008.04.016

[15] Ilie, N. and Hickel, R. (2009) Macro-, Micro- and Nano-Mechanical Investigations on Silorane and Methacrylate-Based Composites. *Dental Materials*, **25**, 810-819. https://doi.org/10.1016/j.dental.2009.02.005

[16] Smith, D.C. (1968) A New Dental Cement. *British Dental Journal*, **124**, 381-384.

[17] Mizrahi, E. and Smith, D.C. (1969) The Bond Strength of a Zinc Polycarboxylate Cement. Investigations into the Behaviour under Varying Conditions. *British Dental Journal*, **127**, 410-414.

[18] Wilson, A.D., Kent, B.E., Clinton, D. and Miller, R.P. (1972) The Formation and Microstructure of Dental Silicate Cements. *Journal of Materials Science*, **7**, 220-238. https://doi.org/10.1007/bf02403512

[19] Strang, R., Whitters, C.J., Brown, D., Clarke, R.L., Curtis, R.V., Hatton, P.V., *et al*. (1998) Dental Materials: 1996 Literature Review. *Journal of Dentistry*, **26**, 191-207. https://doi.org/10.1016/s0300-5712(97)00063-8

[20] Sanchez, P. (2013) Phillips' Science of Dental Materials—Phillip Anusavice. https://www.academia.edu/41764796/Phillips_Science_of_Dental_Materials_Phillip_Anusavice

[21] Wilson, A.D. (1991) Glass-Ionomer Cement Origins, Development and Future. *Clinical Materials*, **7**, 275-282. https://doi.org/10.1016/0267-6605(91)90070-v

[22] Nicholson, J.W. (2002) The Chemistry of Medical and Dental Materials. The Royal Society of Chemistry.

[23] Barandehfard, F., Kianpour Rad, M., Hosseinnia, A., Khoshroo, K., Tahriri, M., Jazayeri, H.E., *et al*. (2016) The Addition of Synthesized Hydroxyapatite and Fluorapatite Nanoparticles to a Glass-Ionomer Cement for Dental Restoration and Its Effects on Mechanical Properties. *Ceramics International*, **42**, 17866-17875. https://doi.org/10.1016/j.ceramint.2016.08.122

[24] Panda, R.N., Hsieh, M.F., Chung, R.J. and Chin, T.S. (2003) FTIR, XRD, SEM and

Solid State NMR Investigations of Carbonate-Containing Hydroxyapatite Nano-Particles Synthesized by Hydroxide-Gel Technique. *Journal of Physics and Chemistry of Solids*, **64**, 193-199. https://doi.org/10.1016/s0022-3697(02)00257-3

[25] Arita, K., Lucas, M.E. and Nishino, M. (2003) The Effect of Adding Hydroxyapatite on the Flexural Strength of Glass Ionomer Cement. *Dental Materials Journal*, **22**, 126-136. https://doi.org/10.4012/dmj.22.126

[26] Clifford, A., Hill, R., Rafferty, A., Mooney, P., Wood, D., Samuneva, B., *et al*. (2001) The Influence of Calcium to Phosphate Ratio on the Nucleation and Crystallization of Apatite Glass-Ceramics. *Journal of Materials Science*: *Materials in Medicine*, **12**, 461-469. https://doi.org/10.1023/a:1011213406951

[27] BS 6039:1981 Specification for Dental Glass Ionomer Cements. https://shop.standards.ie/en-ie/standards/

[28] ISO 9917-1:2007. ISO. https://www.iso.org/standard/45818.html

[29] Young, A.M., Sherpa, A., Pearson, G., Schottlander, B. and Waters, D.N. (2000) Use of Raman Spectroscopy in the Characterisation of the Acid-Base Reaction in Glass-Ionomer Cements. *Biomaterials*, **21**, 1971-1979. https://doi.org/10.1016/s0142-9612(00)00081-8

[30] Barry, T.I., Clinton, D.J. and Wilson, A.D. (1979) The Structure of a Glass-Io Nomer Cement and Its Relationship to the Setting Process. *Journal of Dental Research*, **58**, 1072-1079. https://doi.org/10.1177/00220345790580030801

[31] Bresciani, E., Barata, T.d.J.E., Fagundes, T.C., Adachi, A., Terrin, M.M. and Navarro, M.F.d.L. (2004) Compressive and Diametral Tensile Strength of Glass Ionomer Cements. *Journal of Applied Oral Science*, **12**, 344-348. https://doi.org/10.1590/s1678-77572004000400017

[32] Billingham, J., Breen, C. and Yarwood, J. (1997) Adsorption of Polyamine, Polyacrylic Acid and Polyethylene Glycol on Montmorillonite: An *in Situ* Study Using ATR-FTIR. *Vibrational Spectroscopy*, **14**, 19-34. https://doi.org/10.1016/s0924-2031(96)00074-4

[33] Stoch, L. and Środa, M. (1999) Infrared Spectroscopy in the Investigation of Oxide Glasses Structure. *Journal of Molecular Structure*, **511**, 77-84. https://doi.org/10.1016/s0022-2860(99)00146-5

[34] Huang, C. and Behrman, E.C. (1991) Structure and Properties of Calcium Aluminosilicate Glasses. *Journal of Non-Crystalline Solids*, **128**, 310-321. https://doi.org/10.1016/0022-3093(91)90468-l

[35] Stamboulis, A., Hill, R.G. and Law, R.V. (2005) Structural Characterization of Fluorine Containing Glasses by 19F, 27Al, 29Si and 31P MAS-NMR Spectroscopy. *Journal of Non-Crystalline Solids*, **351**, 3289-3295. https://doi.org/10.1016/j.jnoncrysol.2005.07.029

[36] Hwa, L., Hwang, S. and Liu, L. (1998) Infrared and Raman Spectra of Calcium Alumino-Silicate Glasses. *Journal of Non-Crystalline Solids*, **238**, 193-197. https://doi.org/10.1016/s0022-3093(98)00688-7

[37] Rehman, I. and Bonfield, W. (1997) Characterization of Hydroxyapatite and Carbonated Apatite by Photo Acoustic FTIR Spectroscopy. *Journal of Materials Science*: *Materials in Medicine*, **8**, 1-4. https://doi.org/10.1023/a:1018570213546

[38] Lu, Y. and Miller, J.D. (2002) Carboxyl Stretching Vibrations of Spontaneously Adsorbed and LB-Transferred Calcium Carboxylates as Determined by FTIR Internal Reflection Spectroscopy. *Journal of Colloid and Interface Science*, **256**, 41-52. https://doi.org/10.1006/jcis.2001.8112

[39] Young, A.M. (2002) FTIR Investigation of Polymerisation and Polyacid Neutralisation Kinetics in Resin-Modified Glass-Ionomer Dental Cements. *Biomaterials*, **23**, 3289-3295. https://doi.org/10.1016/s0142-9612(02)00092-3